Nanoscale

PAPER

Cite this: *Nanoscale*, 2015, **7**, 12851

Engineering of the thermodynamic properties of bilayer graphene by atomic plane rotations: the role of the out-of-plane phonons

Alexandr I. Cocemasov,[a,b] Denis L. Nika*[a,b] and Alexander A. Balandin*[a]

Received 31st May 2015,
Accepted 19th June 2015

DOI: 10.1039/c5nr03579a

www.rsc.org/nanoscale

We investigated theoretically the specific heat of graphene, bilayer graphene and twisted bilayer graphene taking into account the exact phonon dispersion and density of states for each polarization branch. It is shown that contrary to a conventional belief the dispersion of the out-of-plane acoustic phonons – referred to as ZA phonons – deviates strongly from a parabolic law starting from the frequencies as low as ~100 cm^{-1}. This leads to the frequency-dependent ZA phonon density of states and the breakdown of the linear dependence of the specific heat on temperature T. We established that ZA phonons determine the specific heat for $T \leq 200$ K while contributions from both in-plane and out-of-plane *acoustic* phonons are dominant for 200 K $\leq T \leq$ 500 K. In the high-temperature limit, $T > 1000$ K, the optical and acoustic phonons contribute approximately equally to the specific heat. The Debye temperature for graphene and twisted bilayer graphene was calculated to be around ~1861–1864 K. Our results suggest that the thermodynamic properties of materials such as bilayer graphene can be controlled at the atomic scale by rotation of the sp^2-carbon planes.

1. Introduction

The discovery of the unusually high thermal conductivity, K, of suspended graphene and few-layer graphene (FLG)[1–4] resulted in a surge of interest in thermal properties of two-dimensional (2-D) materials.[5–15] The optothermal studies conducted with the help of micro-Raman spectroscopy revealed the thermal conductivity $K \sim 2000$–5000 W mK^{-1} (depending on the sample size and quality), near room temperature (RT) for the large graphene samples suspended across trenches in SiO_2 wafers[1–4] or on the transmission electron microscopy (TEM) grids.[5,8] These values are above the bulk graphite limit of $K = 2000$ W mK^{-1} for basal planes at RT.[1] A more recent study using a different experimental technique – electrical thermal bridge – of the residue-free suspended graphene also obtained the thermal conductivity above the bulk graphite limit ($K \sim 2430$ W mK^{-1} at $T = 335$ K).[15] Graphene samples supported on substrates have lower thermal conductivity, *e.g.* $K \sim 600$ W mK^{-1} for graphene on Si/SiO_2 at $T = 300$ K.[6] However, even on a substrate or when embedded in a matrix, FLG reveals higher K as compared to thin films of comparable thickness made of other materials.[1,16]

There is an inherent ambiguity in defining the thermal conductivity of graphene in relation to the thickness value of the atomic plane h (most of studies use $h = 0.35$ nm, which originates from the carbon–carbon bond length). Despite this ambiguity and unavoidable experimental data scatter due to different sizes and quality of the samples, there is a growing consensus among theorists that the phonon thermal properties of graphene can be fundamentally different from those of three-dimensional (3-D) bulk crystals.[1,4,9–11,14,17–22] The latter can be attributed to the 2-D nature of the phonon density of states in graphene and the resulting exceptionally long phonon mean free path (MFP) for the long wavelength phonons. Recent theoretical studies suggested that graphene samples with the 100 μm length[19] or even 1 mm length[20] are required in order to recover the intrinsic thermal conductivity of graphene. In both reports the K values were substantially larger than the bulk graphite limit ($K = 5800$ W mK^{-1} at $T = 300$ K in ref. 19). The specifics of the phonon dispersion and relative contributions of different phonon polarization are important for gaining a complete understanding of thermal properties of 2-D materials.

In this Letter, we report the results of our investigation of the specific heat, c_v, of single layer graphene (SLG), bilayer graphene (BLG) and twisted bilayer graphene (T-BLG). This thermodynamic characteristic can be determined rather accurately

[a]*Nano-Device Laboratory (NDL) and Phonon Optimized Engineered Materials (POEM) Center, University of California – Riverside, Riverside, California 92521, USA. E-mail: balandin@ece.ucr.edu*

[b]*E. Pokatilov Laboratory of Physics and Engineering of Nanomaterials, Department of Theoretical Physics, Moldova State University, Chisinau, MD-2009, Republic of Moldova. E-mail: dlnika@yahoo.com*

and it suffers less from the ambiguity of the phonon transport characteristics. The focus of our present study is on elucidating the role of the out-of-plane phonons in determining the specific heat in different temperature ranges and revealing the influence of the 2-D phonon density of states (PDOS). In addition to a numerical solution we also provide a simple analytical formula for calculating $c_v(T)$ for graphene, BLG and T-BLG with parameters extracted from the Born–von Karman model of the lattice vibrations. We have earlier proposed a possibility of engineering phonon dispersion and material properties by twisting of the atomic planes in T-BLG.[23,24] The first experimental studies of heat conduction in suspended T-BLG confirmed that twisting substantially reduces K owing to the increased scattering phase space available for phonons in T-BLG as compared to the Bernal-stacked BLG.[25] In this Letter the approach for controlling phonon properties at the atomic level by rotating sp^2 carbon planes is treated in a broader context. Knowledge of the specific heat and Debye temperature of SLG, BLG and T-BLG is important for practical applications of these materials as fillers in thermal pastes[26–29] and thermal graphene laminate coatings.[16,30–33]

2. Phonon density of states in SLG, BLG and T-BLG

It is known that SLG reveals four in-plane phonon branches: transverse/longitudinal acoustic (TA/LA) and optic (TO/LO) branches with the atomic displacements in the graphene plane, and two out-of-plane acoustic (ZA) and optic (ZO) branches with the displacements perpendicular to the graphene plane. The in-plane acoustic branches are characterized by the linear energy dispersions over most part of the Brillion zone (BZ) except near the zone edge while the out-of-plane ZA branch demonstrates a quadratic dispersion near the zone center $q = 0$, where q is the phonon wavenumber. The number of phonon branches in BLG is doubled: six additional branches possess non-zero frequency at $q = 0$ and at low frequencies they are affected by inter-layer interactions.[3,10,22,23] The emergence of many folded hybrid phonon branches in T-BLG was explained by the change of the unit cell size and a corresponding modification of the reciprocal space geometry. The number of polarization branches and their dispersion in T-BLG depend strongly on the rotation angle.[23]

We determine PDOS in SLG, BLG and T-BLG using the phonon dispersions calculated in the framework of the lattice dynamics theory. For the intralayer carbon–carbon interaction we use the Born–von Karman (BvK) force constant approach.[23] For the interlayer interaction we use the spherically symmetric interatomic potential with the following components of the force constant matrices: $\Phi^{ij}_{\alpha\beta} = -\delta(r^{ij})r^{ij}_{\alpha}r^{ij}_{\beta}/(r^{ij})^2$, where δ is the force constant of the interlayer coupling; $\vec{r}^{ij}$ is the vector connecting a pair of interacting atoms (i,j); α and β designate the components of the Cartesian coordinates. Since the van der Waals coupling strength between the graphene layers is very weak we model the dependence of the force constant δ on r^{ij} as: $\delta(r^{ij}) = A\exp(-r^{ij}/B)$ with two fitting parameters $A = 573.76$ N m^{-1} and $B = 0.05$ nm,[24] determined by comparison with the experimental phonon frequencies from the Γ–A direction in graphite.[34]

Twisted bilayer graphene can be generated from BLG by rotating, *i.e.* twisting, one layer relative to another by an angle θ in the graphene plane (see Fig. 1(a)). A set of T-BLGs with different rotational angles and commensurate crystal lattice, *i.e.* lattice possessing a translational symmetry, are determined by the following relation:[35] $\cos\theta(p,n) = (3p^2 + 3pn + n^2/2)/(3p^2 + 3pn + n^2)$, where p and n are coprime positive integer numbers. The number of atoms in a unit cell of T-BLG depends on θ and it is given by the relationship: $N = 4(3p^2 + 3pn + n^2)$, if n is not divisible by 3.[23,24] For example, the unit cell of the T-BLG with $\theta(2,1) = 13.2°$ contains 76 atoms and its BZ is 19 times smaller than that of BLG without a rotation (see Fig. 1(b) for BZ sche-

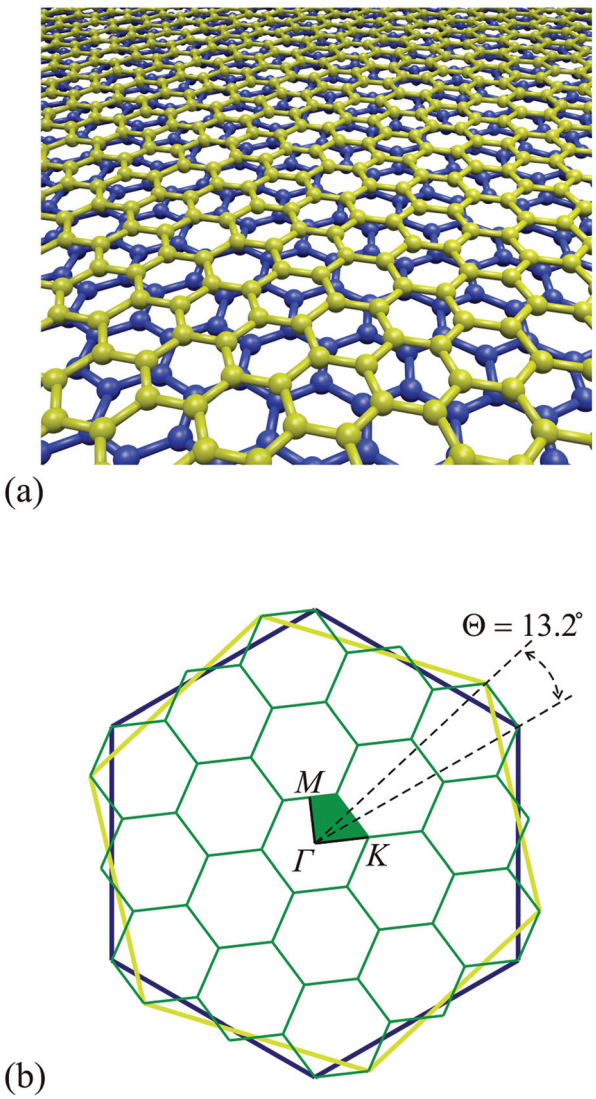

Fig. 1 (a) Twisted bilayer graphene schematics. (b) Brillouin zones of SLG (blue or yellow hexagon) and T-BLG with 13.2° rotation (green hexagon). Γ, M and K denote high-symmetry points of T-BLG BZ.

matics). A detailed description of the theoretical approach for calculating the phonon modes in SLG, BLG and T-BLG was reported by us recently elsewhere.[23,24] Here we use this approach for the investigation of the polarization branch dependent PDOS.

The 2D phonon density of states per unit surface area for SLG and FLG is given by:

$$g(\omega) = \sum_s g_s(\omega);\ g_s(\omega) = \frac{1}{4\pi^2} \sum_{q_x(s,\omega)} \sum_{q_y(s,\omega,q_x)} \frac{\Delta q_x}{|v_y(q_x, q_y, s)|}. \quad (1)$$

Here ω is the phonon frequency, s enumerates phonon branches (polarizations), $g_s(\omega)$ is the polarization-dependent phonon density of states, q_x and q_y are components of the 2D phonon wave vector, $v_y = \partial\omega/\partial q_y$ is the y-component of the phonon group velocity, and Δq_x is the interval between two neighboring q_x points. In order to determine $g(\omega)$ from eqn (1) we calculated $\omega_s(q_x,q_y)$in 40 000 points (q_x,q_y) (200 × 200 grid) uniformly distributed over a 1/4th part of the BZ, shown as a green segment in Fig. 1 for T-BLG with a 13.2° rotation. We checked that increasing the number of points by a factor of 4 does not change the numerical results. Our analysis also showed that 22 500 BZ points (150 × 150 grid) is already sufficient for convergence and obtaining accurate results for PDOS.

The PDOS for LA, TA and ZA branches in graphene can be derived analytically in the isotropic approximation of the linear frequency dispersion for LA and TA branches $\omega_{LA,TA}(q) = v_{LA,TA} \times q$ and quadratic dispersion for the ZA branch $\omega_{ZA}(q) = \alpha \times q^2$ in the entire BZ, where $v_{LA}(v_{TA})$ is the q-independent group velocity and α is a parameter. In this approximation the PDOS per unit surface area takes the form:

$$g^{isot}_{LA,TA}(\omega) = \frac{\omega}{2\pi v^2_{LA,TA}},\ g^{isot}_{ZA}(\omega) = \frac{1}{4\pi\alpha}. \quad (2)$$

The phonon energy dispersion along the Γ–M direction of BZ is shown in Fig. 2 for SLG (panel a), BLG (panel b) and T-BLG with 13.2° rotation (panel c). The red triangles indicate the experimental phonon frequencies of graphite, reproduced from ref. 36. One can conclude that our lattice dynamics model provides a good agreement between the theoretical and experimental phonon frequencies. The dispersion of the ZA branch in SLG and BLG can be divided into two distinctive regions: (I) region with the quadratic dispersion $q < 5.2$ nm^{-1} and (II) region with almost linear dispersion 5.2 nm^{-1} $< q <$ 13.0 nm^{-1}. Therefore we can improve eqn (2) for ZA PDOS accounting for both quadratic and linear dispersion regions:

$$g^{isot}_{ZA}(\omega) = \frac{1}{4\pi\alpha}\Theta(\omega - \omega_c) + \frac{\omega}{2\pi v^2_{ZA}}\Theta(\omega_c - \omega), \quad (3)$$

where ω_c is the phonon frequency separating region (I) from region (II), Θ is the Heaviside's step function and v_{ZA} is the velocity of ZA modes in region II.

In Fig. 3 we analyze partial contribution of LA (green), TA (blue), ZA (red) and ZO (magenta) branches to the total PDOS

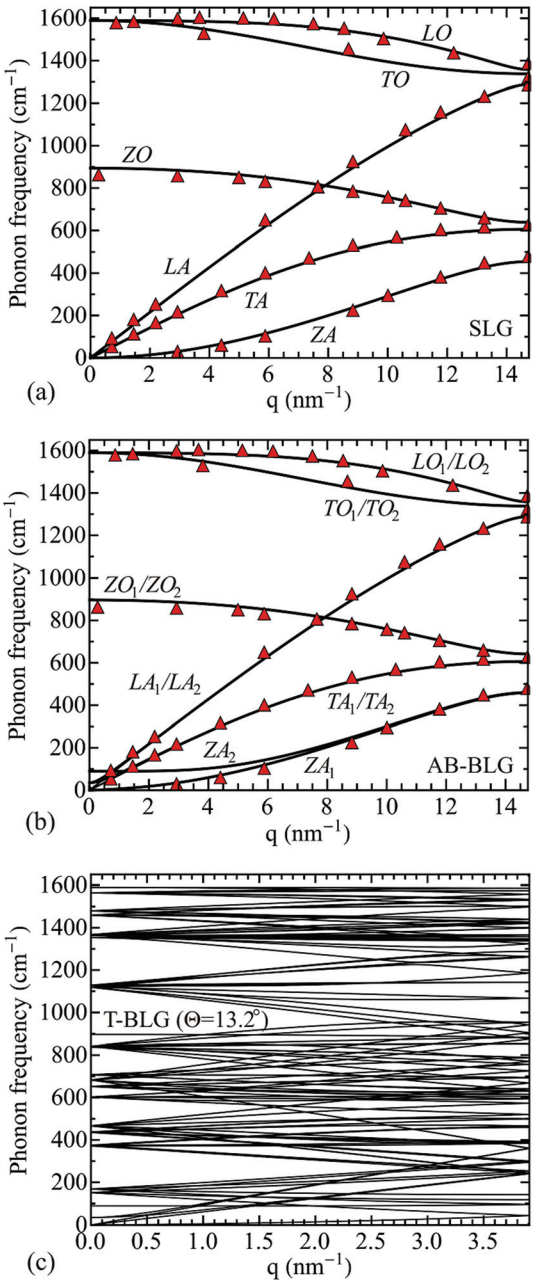

Fig. 2 Phonon dispersion along the Γ–M crystallographic direction in: (a) single-layer graphene, (b) AB-stacked bilayer graphene and (c) twisted bilayer graphene with 13.2° rotation. The red triangles denote experimental phonon frequencies of graphite from ref. 36.

(solid black) for SLG. There are 7 pronounced peaks in the PDOS curve. The peaks at 452, 605 and 638 cm^{-1} are associated with ZA, TA and ZO phonons at the BZ edge, correspondingly. The peak frequency of LA branch ~1192 cm^{-1} is smaller than the LA phonon frequency at M point ~1287 cm^{-1} (see Fig. 2(a)). The main contributors to this peak are the low-velocity phonons from the directions near the BZ edge. The PDOS peak at 889 cm^{-1} is related to the ZO phonon at the BZ center (Γ-point), while TO and LO phonons at the BZ center and the

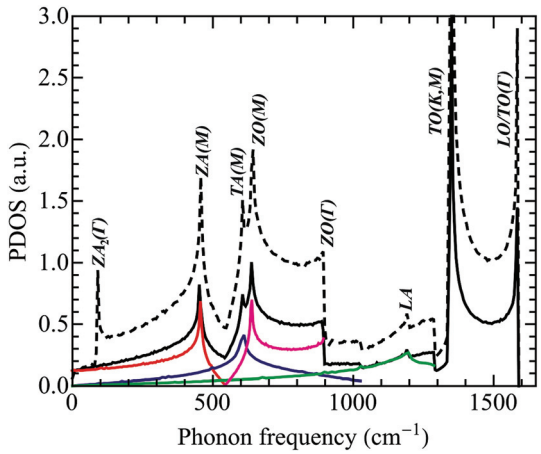

Fig. 3 Total phonon density of states in SLG (solid black) and AB-BLG (dashed black), and contributions from ZA (red), TA (blue), ZO (magenta) and LA (green) phonon branches.

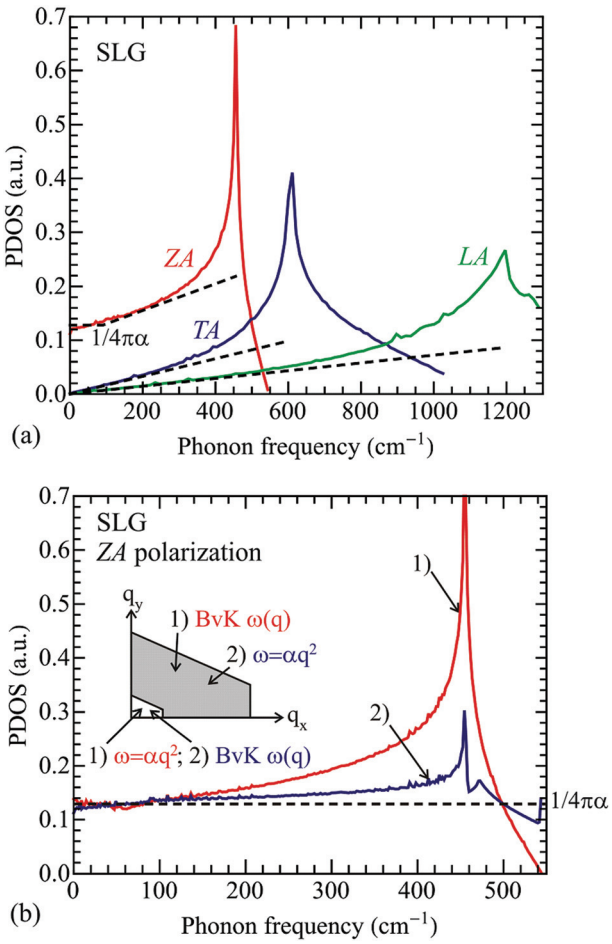

Fig. 4 (a) LA, TA and ZA PDOS calculated from eqn (1), using actual phonon dispersions (solid lines) and obtained in the isotropic model from eqn (2) and (3) (dashed lines). (b) ZA phonon density of states in SLG as a function of phonon frequency calculated using different sets of phonon dispersions.

BZ edge are responsible for peaks at 1350 and 1585 cm^{-1}. In the case of AB-stacked BLG all phonon branches except ZA become nearly doubly degenerated over the entire BZ and the intensity of PDOS is by a factor of ~2 larger than in SLG (see the dashed black line in Fig. 3). The new peak at 91 cm^{-1} also appears in AB-BLG. This peak is associated with the ZA_2 phonon at the Γ-point (see Fig. 2(b)). In T-BLG the frequency of the ZA_2 phonon at the Γ-point depends on the angle of rotation due to the changes in the interlayer coupling,[23] while the overall $g(\omega)$ remains the same as for AB-BLG with a slightly shifted ZA_2 peak. For example, the ZA_2 peak shifts to 89.3 cm^{-1} for T-BLG with 13.2° rotation and to 89.5 cm^{-1} for T-BLG with 21.8° rotation.

In Fig. 4(a) we compare the accurate LA, TA and ZA PDOS in SLG calculated from eqn (1) (solid lines) with those obtained in the isotropic approximation using eqn (2) and (3) (dashed lines). The parameters of the isotropic approximation were extracted from the actual phonon dispersions: υ_{TA} = 13.5 km s^{-1}, υ_{LA} = 20.4 km s^{-1}, υ_{ZA} = 7.9 km s^{-1}, α = 0.62 × 10^{-6} m^2 s^{-1} and ω_c = 90 cm^{-1}. At small energies both sets of the curves almost coincide. The rise of the phonon energy leads to the increasing difference between the curves due to deviation of LA/TA dispersion from the linear law and ZA dispersion from the quadratic law. It is evident from Fig. 4(a), that the high PDOS peaks cannot be described by the isotropic analytical expressions of eqn (2) and (3), and the deviation from the accurate PDOS curves become significant for the frequencies above ~250 cm^{-1} for ZA, ~300 cm^{-1} for TA and ~600 cm^{-1} for LA polarizations. The strong influence of non-parabolicity of the ZA branch on ZA PDOS is illustrated in Fig. 4(b). We show ZA PDOS as a function of the phonon frequency for two cases: (1) a small segment near the BZ center is described by the isotropic and parabolic dispersions while in the rest of BZ the PDOS is calculated using the actual phonon dispersion obtained from BvK model of lattice vibrations (anisotropic and non-parabolic ZA dispersion), and (2) a small segment near the BZ center is anisotropic while the rest is isotropic, which is opposite to case (1).

The difference between the two cases is only in the phonon dispersions used. Both $g(\omega)$ curves were calculated from eqn (1). In the frequency range where the dispersion is parabolic, $g(\omega)$ should be constant and equal to $1/(4\pi\alpha)$ (see eqn (2)). The maximum ZA phonon frequency in the small segment near the BZ center, shown as a white tetragon in Fig. 4, is ~100 cm^{-1} and is almost the same for the parabolic and BvK dispersions. Both $g(\omega)$ curves (red and blue) are practically independent of ω up to ~90 cm^{-1} and coincide with the dashed line $\omega = 1/(4\pi\alpha)$. Therefore, one can conclude that in the region of the phonon wave vectors not far from the BZ center (ω < 90 cm^{-1}) the ZA BvK phonon dispersions are almost parabolic and isotropic. For higher phonon frequencies the difference between the two curves reinforces due to the strong anisotropy and non-parabolicity of the ZA branches.

The Debye temperature is one of the most important parameters describing the thermal properties of solids. We can

estimate the Debye temperature in SLG, BLG and T-BLG, using eqn (1)–(3). In the Debye model the total number of phonon states N_S is given by:

$$N_S = A \sum_{s=\mathrm{LA,TA,ZA}} \int_0^{\omega_\mathrm{D}} g_s^{\mathrm{isot}}(\omega)\mathrm{d}\omega = A(R_1\omega_\mathrm{D}^2 + R_2), \qquad (4)$$

where A is the surface area, $R_1 = \sum_{s=\mathrm{LA,TA,ZA}} 1/\left(4\pi v_s^2\right)$ and $R_2 = \frac{\omega_\mathrm{c}}{4\pi\alpha}\left(1 - \frac{\alpha\omega_\mathrm{c}}{v_\mathrm{ZA}^2}\right)$. Summation in eqn (4) is performed over all acoustic branches. The contribution from the optical phonons is assumed to be zero in the Debye model. Using real PDOS, described by eqn (1), N_S takes the form:

$$N_S = A \sum_s \int_{\omega_{s,\min}}^{\omega_{s,\max}} g_s(\omega)\mathrm{d}\omega. \qquad (5)$$

Here s enumerates both the acoustic and optical phonon branches. From eqn (4) and (5) one can calculate Debye's frequency as:

$$\omega_\mathrm{D} = \sqrt{\frac{\sum_s \int_{\omega_{s,\min}}^{\omega_{s,\max}} g_s(\omega)\mathrm{d}\omega - R_2}{R_1}}. \qquad (6)$$

From eqn (6) we estimated the Debye frequency in SLG, BLG and T-BLG. The Debye frequency is extremely high in all cases and differs rather weakly in SLG, BLG and T-BLG: ω_D(SLG) = 1294.1 cm^{-1}, ω_D(BLG) = 1293.7 cm^{-1} and ω_D(T-BLG) = 1295.7 cm^{-1}, respectively. The weak dependence of ω_D on the number of atomic layers and twisting is an expected result since the main difference between phonon properties of SLG, BLG and T-BLG is due to ZA modes with frequencies $\omega \ll \omega_\mathrm{D}$. These modes are completely populated at temperatures much lower than the Debye temperature $T_\mathrm{D} = \hbar\omega_\mathrm{D}/k_\mathrm{B}$, where k_B and $\hbar$ are Boltzmann's and reduced Planck's constants, respectively; T_D(SLG) = 1862 K, T_D(BLG) = 1861 K and T_D(T-BLG) = 1864 K. These values of T_D exceed those for most of the materials and are only slightly smaller than T_D of diamond ~2000 K.[37]

For comparison, in Table 1 we provide values of T_D for graphite and graphene available in the literature. The separate in-plane and out-of-plane Debye temperatures were calculated from the Debye frequencies using eqn (6) by summation over the in-plane or out-of-plane branches, respectively. The obtained values are in the same range as those calculated for graphite and graphene in ref. 41 and 44 using the lattice dynamics[41] and Green's function theory.[44] At the same time, the smaller values of T_D = 1495 K and 1045 K were estimated experimentally in ref. 42 and 43. We attribute the discrepancy between the theoretical and experimental data to the variations in the contribution of the out-of-plane phonons due to the specific conditions of the experiments.[42,43] For example, authors of ref. 43 assumed that the weak interlayer bonds between graphene and ruthenium substrate modes effectively scatter the impinging He atomic beam when collecting diffraction spectra.

To analyze the influence of the selected inter-layer atomic potentials on the obtained results we performed calculation of PDOS and Debye's temperatures using the Lennard-Jones (LJ) interatomic potential. Although this potential underestimates the phonon energies of bulk graphite in the Γ–A BZ direction,[24] the effect on both PDOS and Debye's temperature is weak. For instance, using LJ potential we obtained the following values of Debye's temperatures in T-BLG (13.2°), which are very close to those obtained using spherically-symmetric potential (see Table 1): $T_\mathrm{D,LJ}$(in-plane) = 2672 K and $T_\mathrm{D,LJ}$(out-plane) = 1293 K.

Table 1 Debye's temperatures in graphene, few-layer graphene and graphite

	T_D (K)	Comment	Ref.
Graphite	1860	Theory: projector augmented wave method + local density approximation	38
	2300 (in-plane) 800 (out-of-plane)	Theory: from fitting the thermal expansion coefficient to experimental data	39
	2300 (in-plane) 800 (our-of-plane)	Theory: from fitting the thermal expansion coefficient to experimental data	40
	2500 (in-plane) 950 (out-of-plane)	Theory: lattice dynamics; from fitting the specific heat to experimental data	41
Graphene	1495	Experiment: suspended and supported	42
	1045	Experiment: supported	43
	2300 (in-plane) 1287 (out-of-plane)	Theory: green functions	44
	1862 2669 (in-plane) 1292 (out-of-plane)	Theory: BvK lattice dynamics; from PDOS comparison	This work
BLG	1861 2675 (in-plane) 1295 (out-of-plane)	Theory: BvK lattice dynamics; from PDOS comparison	This work
T-BLG (13.2°)	1864 2671 (in-plane) 1293 (out-of-plane)	Theory: BvK lattice dynamics; from PDOS comparison	This work

3. Specific heat of SLG, BLG and T-BLG: impact of PDOS

The phonon density of states is a key parameter determining the phonon-assisted processes in graphene and related materials. Knowing the frequency distribution of the polarization-specific PDOS we can address particularly interesting questions: (1) how the phonons of different polarizations determine the functional dependence of phonon specific heat on the temperature and (2) how this dependence changes while going from SLG to BLG and from BLG to T-BLG? The phonon specific heat at a constant volume c_V is given by the following expression:[45,46]

$$c_V(T) = \sum_s c_{s,V}(T);\ c_{s,V}(T) = \frac{3N_A}{k_B T^2}\int_{\omega_{s,\min}}^{\omega_{s,\max}} \frac{\exp\left(\frac{\hbar\omega}{k_B T}\right)}{\left[\exp\left(\frac{\hbar\omega}{k_B T}\right)-1\right]^2}[\hbar\omega]^2 f_s(\omega)\mathrm{d}\omega, \quad (7)$$

where $\omega_{s,\min}(\omega_{s,\max})$ is the minimum (maximum) phonon frequency for the s-th branch, s enumerates phonon branches, T is the temperature, N_A is the Avogadro constant, $f_s(\omega) = g_s(\omega)/\sum_j \int_{\omega_{j,\min}}^{\omega_{j,\max}} g_j(\omega)\mathrm{d}\omega$ is the two-dimensional normalized PDOS and $c_{s,V}$ is the contribution to total specific heat from the s-th branch. Analyzing eqn (7) one can conclude that in the isotropic case of parabolic ZA dispersion $\omega_{ZA} \sim q^2$ and in the case of linear LA/TA dispersions $\omega_{LA,TA} \sim q$, leading to $g_{ZA}(\omega)$ = const and $g_{LA,TA}(\omega) \sim \omega$, the low-temperature specific heat $c_{ZA,V}$ demonstrates the linear dependence on T, while $c_{LA,V}(c_{TA,V})$ scales with temperature as T^2. At very low temperatures, ZA phonons are mostly populated and c_V is proportional to T. Such temperature dependence of specific heat was reported in ref. 47 for T < 100 K. Alofi and Srivastava[48] have theoretically shown that a slight deviation from the linear T dependence occurs due to LA and TA phonon contribution, and $c_V \sim T^{1.1}$ up to 100 K. However, we have recently established[24] that the anisotropy in the phonon dispersions significantly influences the temperature dependence of specific heat in SLG: $c_V \sim T$ for $T \leq 15$ K; $c_V \sim T^{1.1}$ for 15 K < $T \leq$ 35 K; $c_V \sim T^{1.3}$ for 15 K < $T \leq$ 35 K and $c_V \sim T^{1.6}$ for 75 K < $T \leq$ 240 K. For BLG and T-BLG with 21.8° rotation the dependences $c_V \sim T^{1.3}$ and $c_V \sim T^{1.6}$ were revealed correspondingly for T < 15 K. These results require a detailed analysis of the interplay between the accurate phonon energy spectra, PDOS and specific heat, which has not been performed to date.

In Fig. 5(a) the temperature dependences of the phonon specific heat $c_{s,V}$ in SLG are shown for different phonon branches: ZA (red), TA + LA (blue) and ZO + TO + LO (green). The contribution of ZA phonons to c_V is dominant up to $T \approx$ 200 K. Nevertheless, both $c_{ZA,V}$ and c_V demonstrate deviation from the linear T-dependence beginning from $T \approx$ 15 K. This is a clear manifestation of the anisotropy and non-parabolicity of ZA dispersions. The power index m of T^m-dependence of the

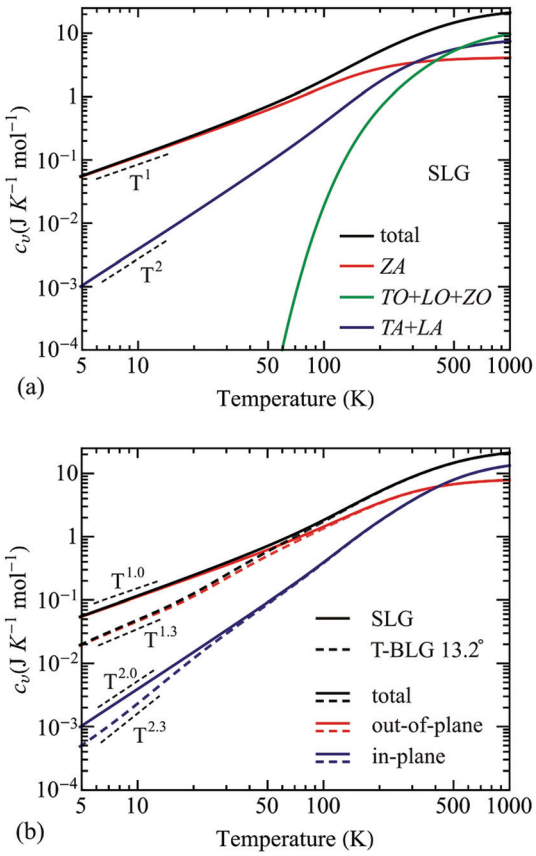

Fig. 5 Phonon branch dependent heat capacity as a function of temperature in SLG (a) and T-BLG with 13.2° rotation (b). In the panel (a) the contributions from different branches are denoted as follows: ZA (red), TO + LO + ZO (green), TA + LA (blue). In the panel (b) the red and blue lines denote contributions from the out-of-plane and in-plane phonons, respectively for SLG (solid curves) and 13.2° T-BLG (dashed curves). In both panels the black curves correspond to the total phonon heat capacity.

specific heat increases faster for total c_V than for $c_{ZA,V}$ due to the contributions from LA and TA phonons revealing $c_{LA,V}(c_{TA,V}) \sim T^2$ dependence for T < 100 K. The contribution of the in-plane phonons to the total c_V increases with temperature and becomes comparable to that of ZA phonon contribution for $T \approx$ 250–300 K. This result differs substantially from what is predicted in the framework of the semi-continuum theory for phonon dispersion where the ratio $c_{ZA,V}/(c_{LA,V} + c_{TA,V}) \sim 2$ was reported for T = 300 K,[48] which was obtained assuming constant PDOS for ZA phonons and linear PDOS for LA and TA phonons. The latter illustrates that the simplified isotropic models for PDOS in graphene do not capture all the characteristics of the specific heat and thermal conductivity. For temperatures $T \geq$ 300 K the contribution of the in-plane acoustic phonons to c_V is larger than that of ZA phonons. The ratio between their contributions $(c_{LA,V} + c_{TA,V})/c_{ZA,V}$ increases from ~1 at T = 300 K to ~1.8 at T = 1000 K. The contribution from optic phonons $c_{op,V} = c_{LO,V} + c_{TO,V} + c_{ZO,V}$ is very small (<10%)

up to $T \approx 180$ K due to the low population of these modes. However, their contribution to c_V increases quickly with temperature: at RT it constitutes ~23%, at $T = 500$ K it is ~36%, while at $T = 1000$ K it is ~46%.

In Fig. 5(b) we illustrate the contribution from the out-of-plane (red lines) and in-plane (blue lines) phonon modes to the total phonon specific heat of SLG (solid lines) and T-BLG with 13.2° rotation (dashed lines) as a function of temperature. The black lines denote the temperature dependence of the total phonon heat capacity in SLG and T-BLG. The specific heat of the out-of-plane phonons varies with temperature as T^m, where $m = 1$ for SLG and $m = 1.3$ for T-BLG at $T < 15$ K. The difference in p is explained by the specifics of the folded phonons in T-BLG (see Fig. 2(c)). In general, the dispersion relations of the "additional" acoustic phonons (denoted as ZA_2 in the case of non-twisted BLG (see Fig. 2(b)) cannot be described by a parabolic law, even at the phonon wave vectors near the BZ center. As a result both p(T-BLG) = 1.3 and p(AB-BLG) = 1.6 (not shown in Fig. 5) are larger than p(SLG). The contribution from the in-plane polarizations to c_V also differs in SLG and T-BLG. At low T in SLG $c_V(T) \sim T^2$, while in T-BLG $c_V(T) \sim T^{2.3}$. This deviation is also due to the appearance of the additional phonon branches in T-BLG with the dispersion relationship different from those in SLG.

The results for T-BLG with the rotational angles other than 13.2° (not shown in Fig. 5) are quite similar, because the difference in the absolute values of the total phonon heat capacity for different BLG configurations at temperatures above 5 K is less than 5% and decreases fast with increasing temperature.[24] The low-temperature specific heat of graphite follows the cubic law $c_V(T) \sim T^3$ due to the three-dimensional density of states, thus increasing the number of graphene layers should increase the power factor m in $c_V(T) \sim T^m$ dependence.

The accurate dependence of the specific heat of SLG, BLG and T-BLG on temperature can be adequately approximated by a parabolic function $c_V(T) = aT + bT^2$, where a and b are constants. The extracted values of these constants for two regions of the temperature $T < 150$ K and 200 K $\leq T \leq$ 350 K are presented in Table 2. In the case of BLG and T-BLG the values of parameters a and b are close, a(BLG) ≈ a(T-BLG), b(BLG) ≈ b(T-BLG), and strongly differ from those of SLG. At low temperatures $T < 150$ K, the ratio b/a in BLG/T-BLG is by a factor of ~6.5 larger than that in SLG, indicating a stronger deviation of BLG/T-BLG ZA dispersions from the parabolic law. The difference between the b/a ratios in SLG and BLG/T-BLG practically disappears at higher temperatures of 200 K $\leq T \leq$ 350 K: b/a (SLG) ~ 0.0018 K^{-1} and b/a(BLG/T-BLG) ~ 0.0019 K^{-1}, where the relative contribution of ZA modes to the specific heat decreases.

Table 2 Constants of parabolic functions $aT + bT^2$ approximating specific heat in SLG, BLG and 13.2° T-BLG

	a ($\times 10^{-3}$ J K^{-2} mol^{-1})	b ($\times 10^{-5}$ J K^{-3} mol^{-1})
$T < 150$ K		
SLG	11.87	7.21
BLG	3.641	13.85
13.2° T-BLG	3.494	13.84
200 K $\leq T \leq$ 350 K		
SLG	19.12	3.42
BLG	18.56	3.57
13.2° T-BLG	18.36	3.6

4. Discussion: controlling phonons at the atomic scale

The obtained results show that ZA phonons dominate the specific heat for $T \leq 200$ K while their contribution becomes comparable to that of LA and TA phonons in the temperature range 200 K $\leq T \leq$ 500 K. In this sense, the out-of-plane vibrations, which resemble standing waves, are efficient in storing thermal energy. However, this does not imply that ZA phonons make the dominant contribution to the thermal conductivity. In the kinetic theory, the phonon thermal conductivity can be written as $K \sim c_V V \Lambda$, where V is the phonon group velocity, $\Lambda = V\tau$ is the phonon MFP and τ is the combined relaxation time of the phonons. The thermal conductivity, particularly near RT, is affected strongly by the phonon group velocity (defined by the slopes of the dispersion branches) and phonon scattering due to inharmonicity of the crystal lattice and defects. The question of the relative contribution of ZA, LA and TA phonons in different temperature ranges and under different conditions (*e.g.* supported graphene *vs.* suspended) is a subject of interesting theoretical debates.[4,10,11,21,49–52] No conclusive experimental evidence has so far been provided.

We have earlier proposed a possibility of controlling heat flow by engineering phonon dispersion in T-BLG.[23,53] The initial experimental studies of thermal conductivity suspended T-BLG performed using the optothermal technique confirmed that twisting substantially reduces K as compared to BLG.[25] The fundamental difference of phonon engineering by twisting from earlier approaches that involved phonon confinement in acoustically mismatched nanostructures, *e.g.* conventional quantum wells and nanowires,[53–58] is a possibility of controlling not only acoustic phonons but optical phonons as well. The twisting of atomic planes results in breaking the unit cells and reducing BZ, which results in the phonon dispersion modification all the way to the optical branch (see Fig. 2(c)). Our present results indicate that SLG, BLG and T-BLG have distinguishably different c_V temperature dependence that can be traced to the PDOS of individual polarization branches. These dependences, which we provided in the analytical form as well, may help in future experimental studies. The possibility of engineering of the acoustic and optical phonon dispersion can be useful for energy storage and thermal management applications.[29]

5. Conclusions

We theoretically investigated the phonon density of states for different phonon branches in single-layer, bilayer and twisted bilayer graphene in the framework of the Born–von Karman model. The density of states for LA, TA and ZA phonons have been compared with those obtained in the simplified isotropic model with the linear dispersion for LA and TA branches and quadratic dispersion for the ZA branch. Our results show that the isotropic model describes well only the low-frequency part of PDOS with $\omega < 250$ cm^{-1} for ZA, $\omega < 300$ cm^{-1} for TA and $\omega < 600$ cm^{-1} for LA modes. The deviation of the out-of-plane acoustic phonon dispersions from the parabolic law breaks the linear dependence of the specific heat on temperature: in SLG c_V(SLG) $\sim T$ only for $T < 15$ K, while specific heat of BLG and T-BLG demonstrates T^n dependence with $n > 1$ even at small temperatures ~1 K. The partial contribution of the different phonon branches to specific heat is a function of temperature: at $T < 200$ K the main contributors are ZA phonons; in the range 200 K–500 K, specific heat is determined by LA, TA and ZA phonons, while at $T > 500$ K the contribution of optic phonons exceeds 35%. We have found that T-dependence of the heat capacity in SLG, BLG and T-BLG can be approximated by a function $aT + bT^2$ at $T < 350$ K and have determined parameters a and b by fitting the accurate $c_V(T)$ curves. The presented results confirm that the accurate phonon density of states is required for both qualitative and quantitative description of the specific heat of SLG, BLG and T-BLG. The dominance of ZA phonons in determining the specific heat for $T \leq 200$ K does not imply their leading role in heat conduction, which depends on the phonon mean free path as well. Our results indicate that the thermodynamic properties of bilayer graphene can be controlled at the atomic scale by rotation of the atomic planes.

Acknowledgements

This work was supported as part of the Spins and Heat in Nanoscale Electronic Systems (SHINES), an Energy Frontier Research Center funded by the U.S. Department of Energy, Office of Science, Basic Energy Sciences (BES).

References

1 A. A. Balandin, *Nat. Mater.*, 2011, **10**, 569–581.
2 A. A. Balandin, S. Ghosh, W. Bao, I. Calizo, D. Teweldebrhan, F. Miao and C. N. Lau, *Nano Lett.*, 2008, **8**, 902–907.
3 S. Ghosh, W. Bao, D. L. Nika, S. Subrina, E. P. Pokatilov, C. N. Lau and A. A. Balandin, *Nat. Mater.*, 2010, **9**, 555–558.
4 D. L. Nika and A. A. Balandin, *J. Phys.: Condens. Matter*, 2012, **24**, 233203.
5 W. Cai, A. L. Moore, Y. Zhu, X. Li, S. Chen, L. Shi and R. S. Ruoff, *Nano Lett.*, 2010, **10**, 1645–1651.
6 J. H. Seol, I. Jo, A. L. Moore, L. Lindsay, Z. H. Aitken, M. T. Pettes, X. Li, Z. Yao, R. Huang, D. Broido, N. Mingo, R. S. Ruoff and L. Shi, *Science*, 2010, **328**, 213–216.
7 Z. Wang, R. Xie, C. T. Bui, D. Liu, X. Ni, B. Li and J. T. L. Thong, *Nano Lett.*, 2011, **11**, 113–118.
8 S. Chen, Q. Wu, C. Mishra, J. Kang, H. Zhang, K. Cho, W. Cai, A. A. Balandin and R. S. Ruoff, *Nat. Mater.*, 2012, **11**, 203–207.
9 D. L. Nika, E. P. Pokatilov, A. S. Askerov and A. A. Balandin, *Phys. Rev. B: Condens. Matter*, 2009, **79**, 155413.
10 L. Lindsay, D. A. Broido and N. Mingo, *Phys. Rev. B: Condens. Matter*, 2011, **83**, 235428.
11 Z. Aksamija and I. Knezevic, *Phys. Rev. B: Condens. Matter*, 2012, **86**, 165426.
12 W.-R. Zhong, M.-P. Zhang, B.-Q. Ai and D.-Q. Zheng, *Appl. Phys. Lett.*, 2011, **98**, 113107.
13 E. Munoz, J. Lu and B. I. Yakobson, *Nano Lett.*, 2010, **10**, 1652–1656.
14 D. L. Nika, A. S. Askerov and A. A. Balandin, *Nano Lett.*, 2012, **12**, 3238–3244.
15 K. Yoon, G. Hwang, J. Chung, H. Kim, O. Kwon, K. D. Kihm and J. S. Lee, *Carbon*, 2014, **76**, 77–83.
16 Z. Yan, G. Liu, J. M. Khan and A. A. Balandin, *Nat. Commun.*, 2012, **3**, 827.
17 S. Lepri, R. Livi and A. Politi, *Phys. Rep.*, 2003, **377**, 1–80.
18 A. Dhar, *Phys. Rev. Lett.*, 2001, **86**, 5882–5885.
19 S. Mei, L. N. Maurer, Z. Aksamija and I. Knezevic, *J. Appl. Phys.*, 2014, **116**, 164307.
20 G. Fugallo, A. Cepellotti, L. Paulatto, M. Lazzeri, N. Marzari and F. Mauri, *Nano Lett.*, 2014, **14**, 6109–6114.
21 L. Lindsay, D. A. Broido and N. Mingo, *Phys. Rev. B: Condens. Matter*, 2010, **82**, 115427.
22 J. Y. Yan, W. Y. Ruan and M. Y. Chou, *Phys. Rev. B: Condens. Matter*, 2008, **77**, 125401.
23 A. Cocemasov, D. L. Nika and A. A. Balandin, *Phys. Rev. B: Condens. Matter*, 2013, **88**, 035428.
24 D. Nika, A. Cocemasov and A. A. Balandin, *Appl. Phys. Lett.*, 2014, **105**, 031904.
25 H. Li, H. Ying, X. Chen, D. L. Nika, A. Cocemasov, W. Cai, A. A. Balandin and S. Chen, *Nanoscale*, 2014, **6**, 13402–13408.
26 K. M. F. Shahil and A. A. Balandin, *Nano Lett.*, 2012, **12**, 861–867.
27 Y.-X. Fu, Z.-X. He, D.-C. Mo and S.-S. Lu, *Int. J. Therm. Sci.*, 2014, **86**, 276–283.
28 M. Zhou, H. Bi, T. Lin, X. Lu, D. Wan, F. Huang and J. Lin, *Carbon*, 2014, **75**, 314–321.
29 J. D. Renteria, D. L. Nika and A. A. Balandin, *Appl. Sci.*, 2014, **4**, 525–547.
30 P. Goli, H. Ning, X. Li, C. Y. Lu, K. S. Novoselov and A. A. Balandin, *Nano Lett.*, 2014, **14**, 1497–1503.
31 H. Malekpour, K.-H. Chang, J.-C. Chen, C.-Y. Lu, D. L. Nika, K. S. Novoselov and A. A. Balandin, *Nano Lett.*, 2014, **14**, 5155–5161.
32 Z. Gao, Y. Zhang, Y. Fu, M. Yuen and J. Liu, *IEEE Trans. Electron Devices*, 2014, **61**, 4171–4175.

33 Z. Gao, *Proc. – Electron. Compon. Technol. Conf.*, 2013, **63**, 2075–2078, DOI: 10.1109/ECTC.2013.6575865.
34 R. Nicklow, N. Wakabayashi and H. G. Smith, *Phys. Rev. B: Condens. Matter*, 1972, **5**, 4951.
35 J. M. B. Lopes dos Santos, N. M. R. Peres and A. H. Castro Neto, *Phys. Rev. B: Condens. Matter*, 2012, **86**, 155449.
36 M. Mohr, J. Maultzsch, E. Dobardžić, S. Reich, I. Milošević, M. Damnjanović, A. Bosak, M. Krisch and C. Thomsen, *Phys. Rev. B: Condens. Matter*, 2007, **76**, 035439.
37 *Graphite and Precursors (World of Carbon)*, ed. P. Delhaes, CRC Press, 2000.
38 T. Tohei, A. Kuwabara, F. Oba and I. Tanaka, *Phys. Rev. B: Condens. Matter*, 2006, **73**, 064304.
39 W. C. Morgan, *Carbon*, 1972, **10**, 73.
40 D. K. L. Tsang, B. J. Marsden, S. L. Fok and G. Hall, *Carbon*, 2005, **43**, 2902.
41 J. Krumhansl and H. Brooks, *J. Chem. Phys.*, 1953, **21**, 1663.
42 M. Pozzo, D. Alfe, P. Lacovig, P. Hofmann, S. Lizzit and A. Baradli, *Phys. Rev. Lett.*, 2011, **106**, 135501.
43 A. Politano, B. Borca, M. Minniti, J. J. Hinarejos, A. L. Vazquez de Parga, D. Farias and R. Miranda, *Phys. Rev. B: Condens. Matter*, 2011, **84**, 035450.
44 V. K. Tewary and B. Yang, *Phys. Rev. B: Condens. Matter*, 2009, **79**, 125416.
45 A. I. Anselm, *Introduction to semiconductor theory*, Mir Publishers, 1981.
46 J. M. Ziman, *Electrons and phonons: the theory of transport phenomena in solids*, Oxford University Press, 2001.
47 V. N. Popov, *Phys. Rev. B: Condens. Matter*, 2002, **66**, 153408.
48 A. Alofi and G. P. Srivastava, *J. Appl. Phys.*, 2012, **112**, 013517.
49 P. G. Klemens, *J. Wide Bandgap Mater.*, 2000, **7**, 332.
50 L. Chen and S. Kumar, *J. Appl. Phys.*, 2012, **112**, 043502.
51 A. Y. Serov, Z.-Y. Ong and E. Pop, *Appl. Phys. Lett.*, 2013, **102**, 033104.
52 L. Lindsay, W. Li, J. Carrete, N. Mingo, D. A. Broido and T. A. Reinecke, *Phys. Rev. B: Condens. Matter*, 2014, **89**, 155426.
53 A. A. Balandin and D. L. Nika, *Mater. Today*, 2012, **15**, 266.
54 A. A. Balandin, *J. Nanosci. Nanotechnol.*, 2005, **5**, 7.
55 A. A. Balandin, E. P. Pokatilov and D. L. Nika, *J. Nanoelectron. Optoe.*, 2007, **2**, 140.
56 D. L. Nika, E. P. Pokatilov and A. A. Balandin, *Appl. Phys. Lett.*, 2008, **93**, 173111.
57 V. A. Fonoberov and A. A. Balandin, *Nano Lett.*, 2006, **6**, 2442.
58 E. P. Pokatilov, D. L. Nika and A. A. Balandin, *Superlattices Microstruct.*, 2003, **33**, 155.